ON HEATING HEAD AND NECK TUMOURS USING THE NOVEL CLINICAL EM APPLICATOR: THE HYPERCOLLAR

M.M. Paulides, J.F. Bakker, E. Neufeld, J. van der Zee,
P.P. Jansen, P.C. Levendag, G.C. van Rhoon

May 2, 2007

Running title: "A clinical H&N applicator prototype"

Abstract

Purpose: Definition of all features and the potential of the novel HYPERcollar applicator system for hyperthermia treatments in the head and neck (H&N) region.
Methods and Materials: The HYPERcollar applicator consists of 1) an antenna ring, 2) a waterbolus system and 3) a positioning system. The specific absorption rate (SAR) profile of this applicator is investigated by performing infra-red (IR) measurements in a cylindrical phantom. Mandatory patient-specific treatment planning is performed as an object lesson to a patient with a laryngeal tumour and an artificial lymph node metastasis.
Results: The comfort tests with healthy volunteers have revealed that the applicator provides sufficient comfort to maintain in treatment position for an hour: in our center the standard hyperthermia treatment duration. We further established that a central focus in the neck can be obtained, with 50% iso-SAR lengths of 3.5cm in transversal directions and 9-11cm in the axial direction (z). Using treatment planning by detailed electromagnetic simulations, we showed that the SAR pattern can be optimized to enable simultaneous encompassing a primary laryngeal tumour and a lymph node metastasis at the 25% iso-SAR level.
Conclusions: A site-specific H&N applicator was designed that enables good control and sufficient possibilities for optimizing the SAR pattern. In an ongoing clinical feasibility study we will investigate the possibilities of heating various target regions in the neck with this apparatus.

Key words: SAR, Treatment planning, Phased-array, Hyperthermia applicator, Head and neck tumours, Electromagnetic.

1 Introduction

Clinical phase III trials have shown that the addition of hyperthermia (HT) to radiotherapy (RT) results in remarkable higher (complete) response rates, improved local control rates, better palliative effects and/or better overall survival rates. The possibilities of HT for improving treatment outcome without adding toxicity [1–5] are interesting to study in also advanced H&N tumours.

Up to now, the application of HT in the H&N region was limited to superficial regions because of the lack of deep-heating equipment for this region [6]. In earlier investigations, phased-array approaches have been investigated to apply HT to superficial regions in the H&N area with planar or conformal arrays [7, 8]. However, to the best of the authors knowledge, no clinical phased-array based applicator for applying HT to deep-seated head and neck tumours exists. Therefore we conducted work to design and construct such an applicator for targeted heating of advanced carcinomas in the H&N region.

In earlier studies, we started with a cylindrically symmetrical setup of dipole antennas in an infinite water environment and optimized the dimensions of this setup specifically for targeted heating in the H&N region [9–11]. In those studies we selected an array of twelve antennas operating at 433MHz arranged in two rings as the optimum setup. Simultaneously, we designed a patch antenna specific for the H&N applicator as a replacement for the dipoles of the theoretical setups [12]. Subsequently, we verified the SAR calculations by phantom measurements using a laboratory prototype consisting of twelve early versions of this patch antenna [13].

The good results in previous studies have led to the construction of a clinical applicator: the HYPERcollar. In the present publication we report on the HYPERcollar applicator system and its features. Further, we show the results of measurements for quality assurance purposes. Finally, as an object lesson, we illustrate the potential of the applicator by showing the mandatory patient-specific treatment planning process for an example larynx-patient, and discussing the predicted optimized SAR distribution.

2 Materials and methods

Three key elements have to be addressed in advance to a semi-deep H&N HT treatment to ensure high quality. Firstly, equipment should be available that provides possibilities for obtaining good specific absorbtion rate (SAR) coverage of the tumour and enable SAR pattern adjustments. Secondly, these SAR patterns should be verified by phantom measurements. Thirdly, patient-specific treatment planning is mandatory to optimize the SAR pattern and diminish the risk of thermally related toxicity. Therefore, in this section, we describe subsequently the HYPERcollar applicator design, and its characteristics, as well as the treatment planning system that is considered an integral element of the applicator.

2.1 Applicator system

Figure 1 shows a picture of the HYPERcollar applicator system. Basically, the system consists of a normal patient-bed and an applicator that can be moved over the head of the patient. After proper positioning, the waterbolus of the applicator is inflated with demineralized water and the twelve coaxial cables of the power system are connected.

2.1.1 Power system

The power system delivers high power radiofrequency (RF) signals with accurately controlled powers ($\pm 5\%$) and phases ($\pm 2^\circ$) to the applicator. First, a Direct Digital Synthesis (DDS) system provides twelve coherent 433.92 MHz signals with independent phase shifts. These signals are amplified with PG70.150.2 power generators (SSB Electronic, Germany)

up to 150W. Circulators protect the amplifiers against reflected power and bi-directional couplers are used to measure both forward and reflected signals. Gains and phases are measured with twelve specially designed detectors [14], which use one of the DDS system signals as a reference. Low-loss (<0.1dB/m) coaxial cables are used to transfer the 433.92MHz signal from the amplifiers to the C-connectors of the antennas.

2.1.2 HYPERcollar

The HYPERcollar consists of a transparent perspex cylinder (radius = 40cm) covered with a fine conducting gauze forming the conducting backplanes required for the patch antennas. Twelve patch antennas in two rings [10] are mounted on the perspex cylinder. The distance between both antenna rings is 6cm. Each patch antenna is connected to a C-female receptacle connector with an extending conducting rod. A brass patch is mounted on this extending rod and a low-dielectric support is added for robustness. Details of the dimensions of the patch can be found in [12]. The entire applicator is attached to a movable trolley and can be rotated around the z-axis (patient-axis) and around the x-axis (left-right) for maximum positioning flexibility. An inflatable waterbolus is attached to the perspex cylinder for cooling of the skin and to enable an efficient transfer of the electromagnetic waves from the antennas into the patient.

2.1.3 Waterbolus system

Figure 2 schematically shows the waterbolus system and a top view of the HYPERcollar: with cross-sections through the patient and waterbolus. The demineralized water in the waterbolus is circulated and temperature controlled by two E4850 refrigerated recirculators (Bio-Rad, Microscience Division). In- and outflow points are located at every other quadrant in order to obtain maximum temperature homogeneity in the waterbolus. A special pump is used to fill the bolus around the patient in approximately 30s and the quick release valve can be used to empty the bolus in less than 5s. A small valve at the top of the applicator is used to remove the air during the filling procedure. By closing all valves, a closed water system is obtained. The recirculators can also be attached to the water vessel to heat or cool this water to the desired water temperature prior to the treatment.

2.1.4 Positioning system

Positioning of the patient in treatment position is carried out as follows. The patient, who is laying on the patient-bed with the head over the edge of the bed, is positioned by moving the applicator as far as possible over the patients head (∼1cm space between shoulders and applicator). Afterwards, the patient is moved to the desired position by altering the height of the patient-bed and subsequently the height of the neck support. Positioning according to planned positions is measured and verified by a special device, including a water-gauge, that enables measurements using the origin of the applicator as a reference. After inflation of the waterbolus, this positioning is verified in order to obtain the highest correspondence to the positions at which treatment planning was performed.

We assessed the level of comfort within the applicator in treatment position using five healthy volunteers, e.g. if easily breathing remains possible. The volunteers were positioned

within the applicator and subsequently the waterbolus was inflated with water. Volunteers remained in the applicator for approximately an hour.

2.2 Characterization measurements

Compared to the laboratory prototype setup [13], the main differences are 1) the presence of a finite waterbolus, 2) a smaller distance between both antenna rings (6cm), 3) a larger ring radius (40cm) and 4) a new, more optimized, version of the patch antenna [12]. For characterization and quality assurance (QA) purposes we measured reflection and SAR patterns. The reflection P_r that is measured at the connectors of the HYPERcollar can be separated into the primary reflection of the antenna $P_{p.r.}$ and the combined secondary contributions $P_{s.c.}$ by cross-coupling of the other antenna elements of the array, i.e. $P_r = P_{p.r.} + P_{s.c.}$, where $P_{s.c.}$ is the sum of the secondary contributions of the other eleven antennas. Dividing these contributions by the power that is directed towards each antenna, P_f, provides the respective reflection coefficients. Primary reflection characteristics were measured for various waterbolus temperatures to assess the temperature range in which operation is possible. The primary reflection coefficients were measured by attaching a network analyser (8751A, Agilent Technologies, USA) to the antennas and by using a centrally positioned cylindrical muscle equivalent phantom [13]. We further assessed the SAR pattern of the HYPERcollar applicator within this cylindrical phantom by infrared (IR) thermography, as in [13]. In addition, we measured the (phase-dependent) total reflection P_r for the phase settings corresponding to TCP steering in x (-60mm : 60mm), y (-60mm : 60mm) and z (-30mm : 30mm) direction, in steps of 10mm.

2.3 Treatment planning

In future, we will perform treatment planning for each patient since in our opinion this is mandatory for obtaining good heating profiles and to diminish the possibility of thermally related toxicity. Therefore, we illustrate such treatment planning for an example patient with a laryngeal tumour. Further, we illustrate the potential of large target volume heating by adding an artificial lymph node metastasis and analyzing the SAR distributions within tumour and lymph node.

2.3.1 Patient model

The patient model was segmented from a CT-scan of a larynx patient that was made for radiotherapy treatment planning. Semi-automatic segmentation into different tissues was carried out by a medical doctor using a dedicated segmentation program [15] (Figure 3). The segmented tumour volume was 6.5ml, which corresponds to the smallest target volume in [9]. To investigate the possibilities of heating both primary tumour and lymph node metastasis, we also defined an artificial tumorous lymph node sphere (ø = 4cm, volume = 33.5ml) and assigned properties of tumour to this volume. Because the CT-scan contained information of only 30cm, we stretched the end slices of this model to increase the height of the model to the outside of the waterbolus. Tissue properties at 433MHz (Table 1) for normal tissues were from Gabriel et al. [16]. The properties of tumour tissue were obtained by using the average di-electric value of a number of tumours as measured by Joines et al. [17].

Table 1: Tissue types and their dielectric properties at 433 MHz ($\mu_r = 1.0$).

Tissue type	ϵ_r [-]	σ_{eff} [S/m]	ρ [kg/m^3]
Air	1	0	0
Bone	13	0.09	1990
Fat	12	0.08	916
Muscle/Tongue	57	0.80	1041
BloodVessel	47	0.57	1060
BoneMarrow	6	0.03	1027
Brain	57	0.75	1039
Cartilage	45	0.60	1100
Esophagus	67	1.01	1040
SpinalCord	42	0.45	1043
ThyroidGland	61	0.89	1050
Tooth	13	0.09	2160
Tumour	59	0.89	1050

2.3.2 Applicator modelling

We predicted the specific absorption rate (SAR) distributions in the clinical prototype applicator using SEMCAD X (Schmid & Partner Engineering AG, Switzerland). Settings for the FDTD modelling of the HYPERcollar were equal as in [13], in which we verified the accuracy of the model for a laboratory prototype. The grid was aligned to the antennas and automatically refined down to 0.5mm at the antennas for maximum accuracy (Figure 4), which resulted in a total amount of 7.8M voxels.

2.3.3 SAR optimization

2.3.4 Measurement procedures and phase settings

TCP settings The first method of SAR steering is in analogy to the method that is used in the BSD2000 Sigma-60 system [13]. For each antenna, we analytically calculated the required phase-delays, using the difference in wave velocity in muscle and water, such that maximum interference occurs at the desired Target Center Point (TCP) in a cylindrical phantom. These phases are subsequently used in the setup with patient anatomy and HYPERcollar. The amplitudes are always equal for all antennas.

Optimized SAR Powers and phases are optimized by using the optimization procedure of Kohler *et al.* [19] to maximize optimization parameter I:

$$I = \frac{\sum_{i=1}^{N_i} \sum_{t_i} S_i \cdot SAR\{x(t_i), y(t_i), z(t_i)\}}{\sum_{j=1}^{N_j} \sum_{n_j} S_j \cdot SAR\{x(n_j), y(n_j), z(n_j)\}}, \tag{1}$$

in which t_i is the i^{th} target region from a total of N_i target regions and n_j is the j^{th} normal tissue region from N_j normal tissue regions. The total amount of SAR in a certain region

can be increased or decreased respectively by increasing specificity factors S_i and S_j.

3 Results

3.1 Comfort of the applicator

Comfort tests with healthy volunteers have revealed that the applicator provides sufficient comfort to maintain in treatment position for an hour: which will be the hyperthermia treatment duration for H&N patients in our center. We observed no breathing problems due to waterbolus pressure at the trachea, provided that the waterbolus was filled carefully. A special neck support has been constructed since the comfort tests revealed that such a support would provide more stability during filling of the waterbolus and would increase the reproducibility of the positioning.

3.2 Characterization measurements

3.2.1 Reflection characteristics

In [12] we have defined the expected clinically relevant range of waterbolus temperatures, i.e. between 20 and 30°C. Figure 5 provides the primary reflection coefficients measured using the NWA at each antenna, for waterbolus temperatures within and outside this range. The figure shows a temperature dependence, related to the change of the permittivity of the water underneath the patch, that is in agreement with the findings in [12]. The primary reflection of almost all antennas is below -15dB (3%) for temperatures between 20 and 30°C. Loosening this threshold to -10dB (10%), the applicable temperature range can even be increased to between 15 and 35°C, while the average reflection coefficient remains under -14dB.

Table 2: Statistics of the measured reflection coefficient P_r/P_f (%) at every antenna for TCP-steering settings.

	1_1	1_2	1_3	1_4	1_5	1_6	2_1	2_2	2_3	2_4	2_5	2_6	Mean
Mean	10	3	5	6	5	6	12	5	3	4	8	3	6
Max	31	15	19	24	28	18	41	19	11	28	20	21	23

Table 2 summarizes the statistics of the measured total reflection coefficient P_r/P_f for the different phase settings. This table shows that, due to primary reflection and secondary contributions, on average 6% reflection can be expected during treatments, with peaks up to around 31%. The reflection values are found to be highest for the most ventral antennas (1_1 and 2_1). This is due to the waterbolus that bulges out more in dorsal (-y) locations than in ventral (+y) locations. Therefore, the water-air transitions are the closest to the antennas and air inclusions, due to the folds in the waterbolus, are the largest.

3.2.2 Measured SAR distribution

By IR measurements we have established that a central focus can be obtained in the cylindrical muscle equivalent phantom. Figure 6 shows the measured SAR pattern for

central steering settings, i.e. TCP=(0,0,0). The figure shows a central focus very close to the desired focus position. The small asymmetry that can be observed in the x-direction falls within the assumed accuracy of the measurement.
The length $L_{50\%}$ of the focus for central steering is around 90mm and its width $W_{50\%}$ is 35mm (Table 3). By TCP based phase adjustments, the focus can be steered to maximum 50mm (x-direction), 50mm (y-direction) and 30mm (z-direction) from the origin (central steering) in the homogeneous muscle equivalent phantom. Table 3 shows that the dimensions of the focus change for steering in the x (and y) direction but remain equal for steering in the z direction, i.e. the focuslength varies between 88 and 103mm and the focuswidth between 35 and 48mm.

Table 3: SAR steering (Direction and TCP setting (x,y,z)) and corresponding focus-size (length $L_{50\%}$ and width $W_{50\%}$ of the 50% iso-SAR contour) parameters for the IR thermography measurements. All dimensions are in mm.

Direction	**TCP setting**	$L_{50\%}$	$W_{50\%}$
Central	(0, 0, 0)	88	35
X-steering	(-30, 0, 0)	103	48
Z-steering	(0, 0,-30)	90	35

3.3 Predicted SAR in a patient model

SAR distributions were evaluated by using the 1g averaged Spatial Peak SAR [IEEE-1529] to remove high SAR values due to the staircase approximation of FDTD. For the SAR predictions corresponding to the different SAR steering settings we show the 25% iso-SAR volume and cumulative SAR-Volume histograms. In stead of normalizing the SAR distributions to the maximum value we calculated the SAR for 1 Watt total input power so absolute SAR values can be obtained by multiplication with the total input power of all combined antennas. Since we used a highly detailed description of the complete patch antennas, including all their dimensions, and we consider only the real radiated power, we consider these results to be predictive for the actual SAR.

3.3.1 25% iso-SAR volumes

The possibilities of TCP based phase-steering and optimized phase and amplitude settings for this patient are shown by Figure 7. The figure shows the 25% iso-SAR volume on top of the tumour, lymph node and bony structures. Figure 7a shows the iso-SAR volumes corresponding to TCP steering with the TCP in the middle between tumour and lymph node ("TCP @ tumour + lymph node"). This results in SAR coverage at the lymph node but the tumour is not covered. Therefore we adjusted the point of focus towards the center of the tumour. The corresponding SAR is shown by Figure 7b ("TCP @ tumour"). For these phase settings a much better coverage of the tumour and an almost equal situation for the lymph node is obtained but at the cost of 1) hotspots at the shoulder and 2) a large region of high SAR values at the back of the neck region. Figure 7c shows the iso-SAR volumes for optimized settings with equal selectivity values for all tissues ("Optimized

settings"). The figures show selective SAR coverage of the lymph node and limited coverage of the more difficult to heat central tumour. Therefore we increased the selectivity value of the tumour (S_tumour) to 10 in order to obtain a better SAR coverage of both tumour and lymph node, which is shown in Figure 7d. This figure shows that the change in priority led to coverage of all of the tumour and almost all of the lymph node by the 25% iso-SAR volume.

3.3.2 Cumulative SAR-Volume histograms

To show the more subtle differences in the SAR patterns of the two optimized settings, we show the cumulative SAR histograms in Figure 8. Histogram curves are shown for tumour, lymph node, central nerve system (CNS: myelum and brains), and total head volume. Figure 8 shows that the SAR level at the CNS tissues (myelum and brain) is low and that, using both settings, the target region can be heated effectively. The SAR values in the lymph node volume, however, are much higher than the SAR values in tumour for equal selectivity settings ($S_{tumour} = S_{lymphnode} = 1$). The SAR coverage of the tumour can be effectively improved by a ten-fold increase of the tumour volume selectivity value, due to lower values in the lymph node and higher values in the tumour. Therefore a much more homogeneous SAR coverage of the entire target region is obtained with these settings, i.e. over 85% of all SAR values in both targets region are above the 25% iso-SAR value.

4 Discussion

Comfort tests with healthy volunteers have revealed that the HYPERcollar provides sufficient stability to remain in treatment position for an hour. Further, we observed no breathing problems due to waterbolus pressure at the trachea, provided that the waterbolus was filled carefully. However, we anticipate that comfort may be lower for patients with a combination of a short neck and high shoulders. Further, we still need to assess if completion of an entire session is possible for the patients that are generally older and may suffer from severely damaged skins. In a clinical feasibility study we will investigate whether these items of concern lead to major problems. In that study we will also investigate whether heating or comfort problems can be solved by a changed applicator design or can be converted into exclusion criteria for selected groups of patients.

The primary reflection coefficients ($P_{p.r.}$) of, early versions of, the twelve patch antennas in the laboratory prototype were all beneath -10dB for waterbolus temperatures at 23°C and 25°C [13]. The newly designed patch antenna [12] is found to perform better, with a maximum primary reflection of -12dB for temperatures between 15°C and 35°C. However, when taking into account the contributions of other antennas we find a total reflected power of maximum 31% and 6% on average, for measurements using a variety of phase settings and with the water temperature at 25°C. Since we expect that cross-coupling is not temperature dependent, we assume that the minor increase in primary reflection results in acceptable reflection values at waterbolus temperatures in the range of 15°C to 35°C. In the clinical applicator, we installed circulators that guide the remaining reflection towards a matched load and, since the amplifiers can deliver sufficient power, we expect is no influence of these reflections on the treatment.

In an earlier study, using a laboratory prototype, we found a central 50% iso-SAR focus of 35mm (±3mm) in diameter and around 100mm (±15mm) in length [13]. However, based on a simultaneously performed parameter study [10], we decreased the distance between the two antenna rings from 8cm to 6cm and increased the antenna ring-radius from 30cm to 40cm for the HYPERcollar applicator. As expected, the width of the 50% iso-SAR focus is equal for prototype and HYPERcollar. The length of this focus, however, decreases a little to 90mm while a small increase was expected. The decrease in focus length is caused by the finite length of waterbolus introducing water-air transitions that were not taken into account in the prototype setup. However, we expect that the waterbolus will conform better to a patient anatomy, that has a larger average diameter and more concave shape, and waterbolus edges will therefore be further away from the region of interest. Therefore, the influence of the waterbolus on the SAR pattern in a patient is expected to be lower than the influence on the phantom. Nevertheless, the waterbolus shape should resemble the actual shape as close as possible for obtaining a good match between the predictions and the reality.

In this study we calculated the SAR for 1 Watt total input power so absolute SAR values were obtained. These SAR values are considered predictive for the actual SAR since we accurately model the entire antenna. In an earlier study, we have shown that using such a model the impedance of the antenna can accurately be predicted using SEMCAD X [12]. Since the field pattern is generally a less sensitive parameter than the impedance for such a patch antenna setup, we assume a high predictability also for the electric field pattern. In that study [12], however, we modelled the complete connector and the transmission line while in the current study we used the commonly accepted approach to apply a voltage source at the gap between the conducting backplane and the rod of the patch antenna. By comparing these ways of modelling, we found no differences in electric field pattern and a scalar difference in power of around 15%.

The possibilities of heating in the neck region has been investigated by performing treatment planning on an example patient with a laryngeal tumour and an artificial lymph node sphere. The tumour of 6.52ml corresponds to the smallest target volume in [9] and may be smaller than the general tumour size of patients suffering from advanced tumours. By adding a relatively large lymph node region at the periphery of the neck we obtained a more difficult to heat target region. It can be seen as an extreme case since SAR coverage was required for a maximum distance of 8.3cm, while it was attempted to achieve a low SAR level in between at the normal tissues. A high SAR at a large target volume means sufficient de-focussing possibilities and a low SAR in between the target volumes requires additional degrees of freedom. We found that selective focussing at the target area can be obtained in the transversal plane but in the direction of the patient axis (z-axis) this focus is somewhat large for target-specific heating. The tumour alignment in the transversal plane is more important since in this planes the critical tissues are nearby. Currently we are performing a clinical feasibility study in which we are investigating the feasibility of selectively heating a target region in the H&N region with the HYPERcollar applicator system.

Thermal predictions were not carried out since: 1) the blood perfusion rate of H&N tumours can vary up to 80-fold [20] and 2) large differences in blood perfusion rate have been measured for increasing temperatures (muscle: 0.45 - 40 kg/m3/s) [21]. A separate analysis containing a thorough sensitivity analysis is required to shine some light on the

obtained temperature distributions. Since our initial aim has always been to design an applicator that provides possibilities to obtain a good SAR coverage of the target volume, we have omitted thermal calculations.

5 Conclusions

The HYPERcollar, a newly constructed H&N HT applicator has been presented and its features has been explained. By tests with healthy volunteers we established that the applicator is sufficiently comfortable for a healthy person to be in treatment position for one hour.

From the characterization measurements we conclude that the reflections remain sufficiently low within a waterbolus temperature range of 15-35°C. By IR thermography we measured a central 50% iso-SAR focus of around 90mm in axial and 35mm in radial direction in a muscle equivalent phantom.

Treatment planning showed that the SAR pattern can be shaped such that simultaneous 25% iso-SAR coverage of a deep-seated tumour and a superficial lymph node is possible for this example case. Future research, applying heat sessions to patients, will be used to verify the possibilities of deep heating of arbitrarily shaped target regions in the H&N area.

Acknowledgements

This work was financially supported by the Dutch Cancer Society, grant: DDHK 2003-2855. The authors further would like to thank B. van Toorn for manufacturing the clinical applicator prototype.

References

[1] El-Sayed S and Nelson N. Adjuvant and adjunctive chemotherapy in the management of squamous cell carcinoma of the head and neck region: a meta-analysis of prospective and randomized trials. *J. Clin. Oncol.* 1996; 14: 838-847.

[2] Pignon JP, Bourhis J, Domenge C, et al. Chemotherapy added to locoregional treatment for head and neck squamous-cel carcinoma: three meta-analyses of updated individual data. *Lancet* 2000; 355: 949-955

[3] Trotti A. Toxicity in head and neck cancer: a review of trends and issues. *Int. J. Radiation Oncology Biol. Phys.* 2000; 47: 1-12.

[4] Valdagni R., Liu F-F. and Kapp S. Important prognostic factors influencing outcome of combined radiation and hyperthermia, *Int. J. Radiat. Oncol. Biol. Phys.* 1988; 15: 959-972.

[5] Valdagni R. and Amichetti M. Report of long-term follow-up in a randomized trial comparing radiation therapy and radiation therapy plus hyperthermia to metastatic lymphnodes in stage IV head and neck patients. *Int. J. Radiat. Oncol. Biol. Phys.* 1993; 28: 163-169.

[6] Stauffer, PR. Evolving technology for thermal therapy of cancer. *Int J Hyperthermia* 2005; 21: 731-744, Review.

[7] Jouvie F, Bolomey JC, Gaboriaud G. Discussion of the capabilities of microwave phased arrays for hyperthermia treatment of neck tumours. *IEEE Trans. Micr. Theor. Tech.* 1986; 34: 495-501.

[8] Magin RL, Peterson AF. Noninvasive microwave phased arrays for local hyperthermia: a review. *Int. J. Hyperthermia* 1989; 5: 429-450.

[9] M.M. Paulides, S.H.J.A. Vossen, A.P.M. Zwamborn and G.C. Van Rhoon, "Theoretical investigation into the feasibility to deposit RF energy centrally in the head and neck region," *Int. J. Rad. Onc. Biol. Phys.*, vol. 63, pp. 634-642, 2005.

[10] M.M. Paulides, J.F. Bakker, A.P.M. Zwamborn, G.C. Van Rhoon, "A head and neck hyperthermia applicator: theoretical antenna array design," *Int. J. Hyperthermia*, vol.23, pp. 59-67, 2007.

[11] M.M. Paulides, D.H.M. Wielheesen, J. Van der Zee and G.C. Van Rhoon, "Assessment of the local SAR distortion by major anatomical structures in a cylindrical neck phantom," *Int. J. Hyperthermia*, vol. 21, pp. 125-140, 2005.

[12] M.M. Paulides, J.F. Bakker, N. Chavannes and G.C. Van Rhoon, "A patch antenna design for a phased-array head and neck hyperthermia applicator," *IEEE Trans. Biom. Eng.*, In press.

[13] M.M. Paulides, J.F. Bakker and G.C. Van Rhoon, "A head and neck hyperthermia applicator: experimental phantom verification and FDTD model," *Int. J. Rad. Onc. Biol. Phys.*, In press.

[14] J.F. Bakker, M.M. Paulides, G.C. van Rhoon, H. Schippers and T.A. Ter Meer, "Development of a gain & phase detector for a hyperthermia applicator", in Proceedings of the joint 9th International Conference on Electromagnetics in Advanced Applications (ICEAA '05) and 11th European Electromagnetic Structures Conference (EESC '05), ISBN 88-8202-094-0, Torino, Italy, 2005: 209-212.

[15] E. Neufeld, T. Samaras, N. Chavannes, N. Kuster. "Robust, highly detailed, medical image segmentation," in the Book of Abstracts of the 22nd Annual Meeting of the ESHO, Graz, Austria (ESHO-05), 2005: 56-57.

[16] S. Gabriel, R.W. Lau and C. Gabriel, "The dielectric properties of biological tissues III: Parametric models for the dielectric spectrum of tissues", *Phys. Med. Biol.*, vol. 41, pp. 2271-2293, 1996.

[17] W.T. Joines, Y. Zhang, C. Li C, R.L. Jirtle. The measured electrical properties of normal and malignant human tissues from 50 to 900 MHz. *Med. Phys.* 1994; 21: 547-50.

[18] SEMCAD: the Simulation platform for EMC, Antenna Design and Dosimetry
Schmid & Partner Engineering AG
http://www.speag.com

[19] T. Kohler, P. Maass, P. Wust and M. Seebass. A fast algorithm to find optimal controls of multiantenna applicators in regional hyperthermia. *Phys. Med. Biol.* 2001; 46: 2503-2514.

[20] P. Vaupel and M. Höckel. Blood supply, oxygenation status and metabolic micromilieu of breast cancers: Characterization and therapeutic relevance (Review). *Int J Oncol* 2000; 17: 869-879.

[21] Lang, J, Erdmann, B and Seebass, M. Impact of nonlinear heat transfer on temperature control in regional hyperthermia. *IEEE Trans Biomed Eng* 1999; 46: 11291138.

Figure 1: Picture of the HYPERcollar applicator system. Both patient bed and positioning system (neck support) are used to position the patient. The coaxial cables, that are normally connected to the applicator, are not shown for visibility.

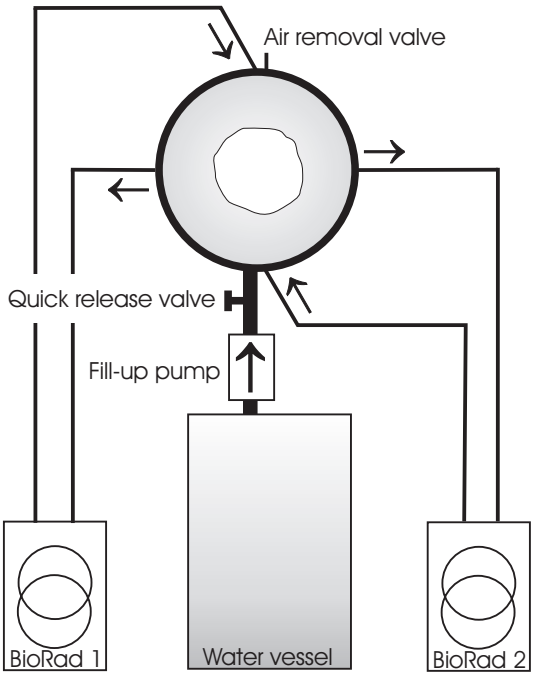

Figure 2: Schematic visualization of the waterbolus system. Direction of flow within the tubes is indicated by the arrows.

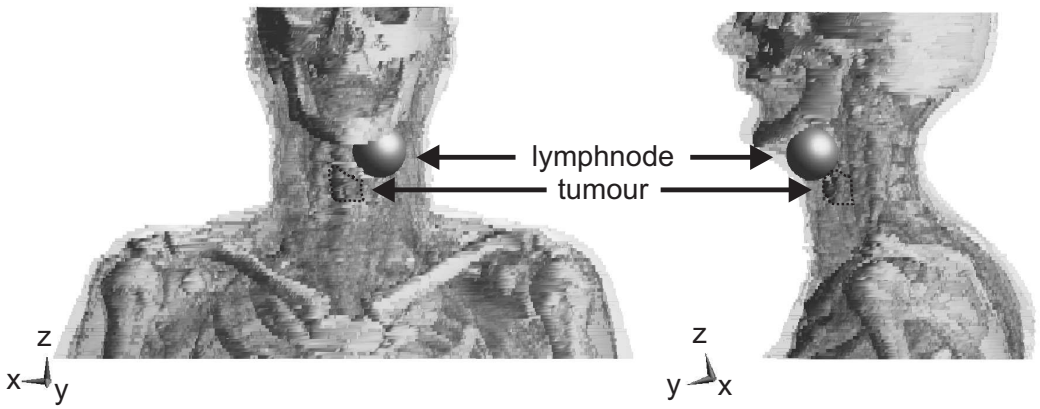

Figure 3: Transparent anatomy visualization in SEMCAD X. Bone tissue, the tumour and the artificial lymph node metastasis are non-transparently visualized.

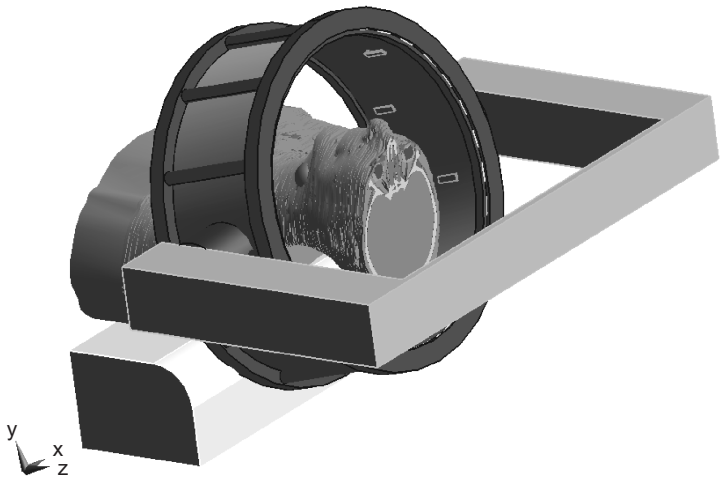

(a): Solid model

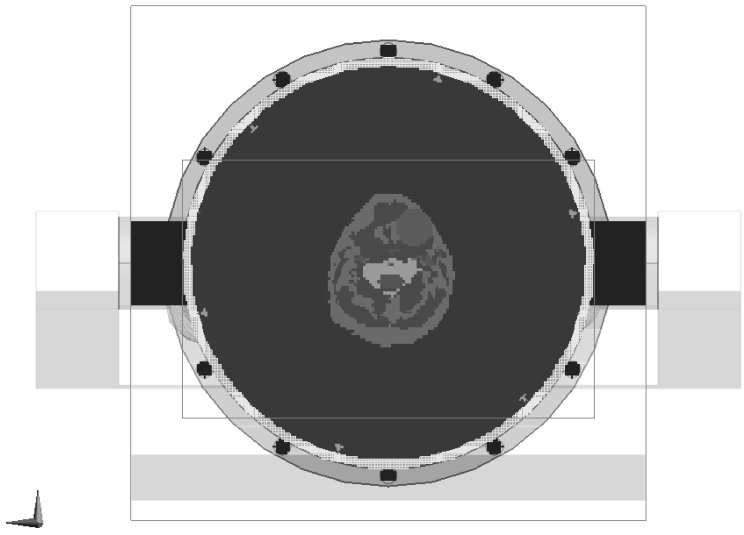

(b): Grid implementation

Figure 4: The HYPERcollar applicator and the patient within. The waterbolus and the head model extension are not visualized to show some patch antennas.

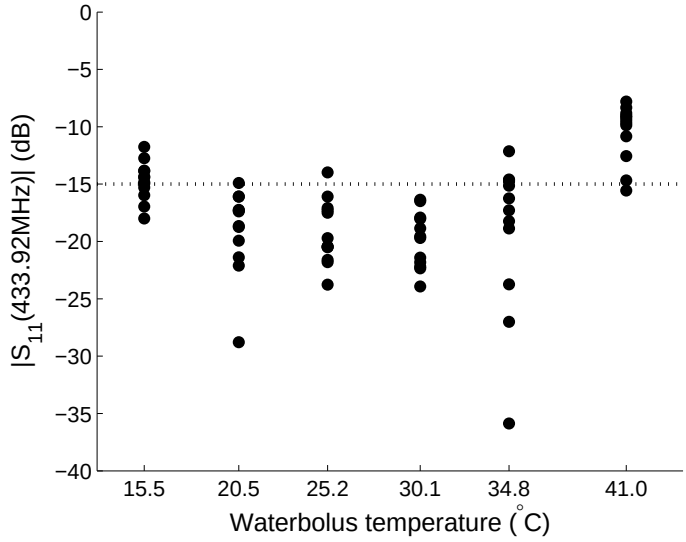

Figure 5: Primary reflection coefficient ($P_{p.r.}/P_f$ in dB) at 433.92MHz for different waterbolus temperatures and all 12 antennas. A cylindrical muscle equivalent phantom was used to mimic the patient's neck.

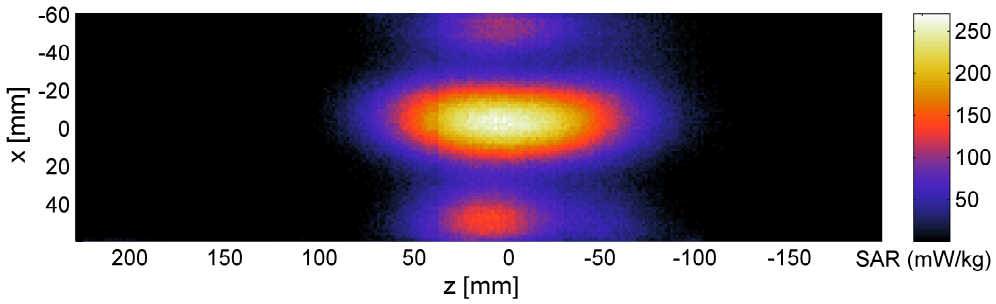

Figure 6: SAR distribution within the, 11.6cm diameter, cylindrical muscle equivalent phantom for central phase steering ($\varphi_i = 0$, $i = 1 \dots 12$) and a combined total input power of 1W.

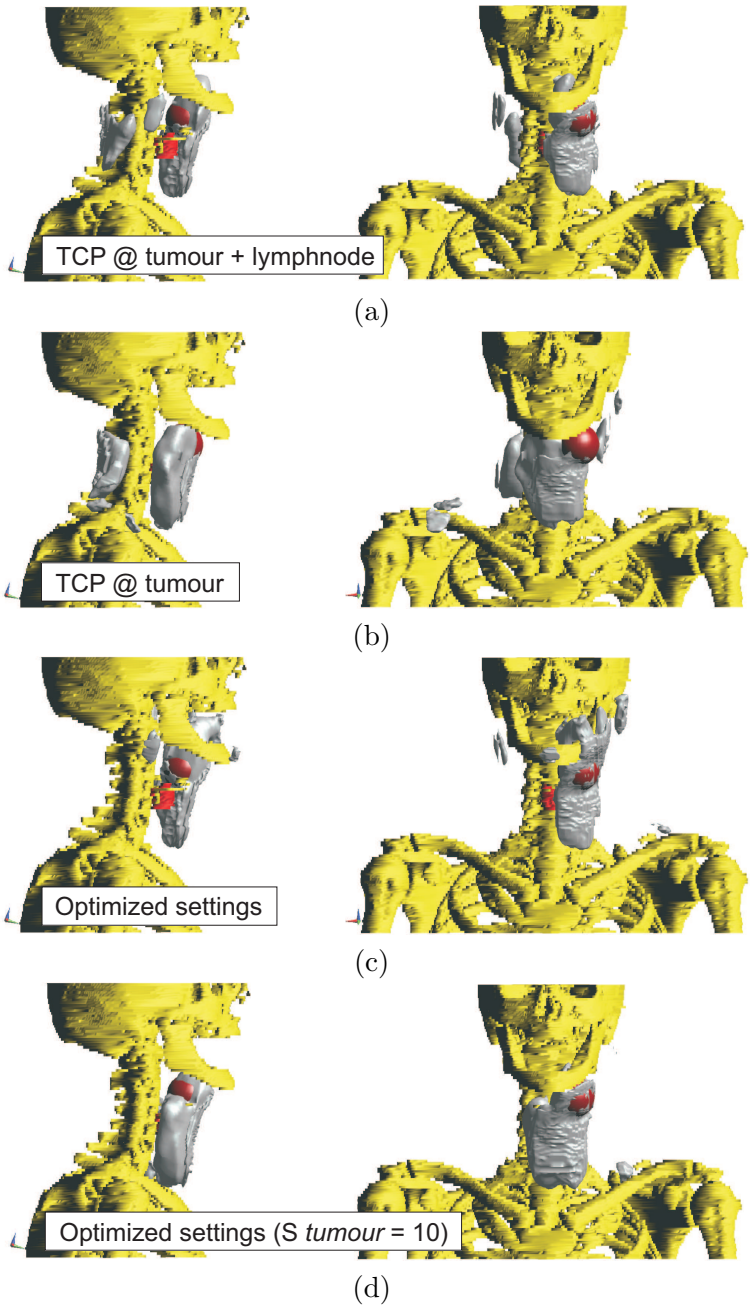

Figure 7: 25% iso-SAR volumes, shown in white, for the four investigated settings. The figure further shows the bony structures (yellow) and the tumour (red) and artificial lymph node sphere (dark red)

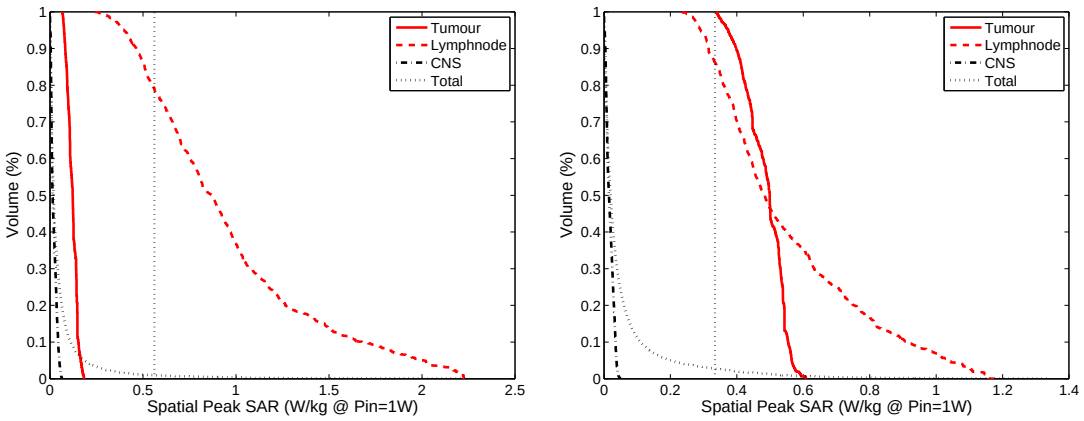

(a) Optimized settings
$S_{tumour} = 1$, $S_{lymphnode} = 1$

(b) Optimized settings
$S_{tumour} = 10$, $S_{lymphnode} = 1$

Figure 8: Cumulative SAR-Volume histograms for optimized phases and amplitudes of the signals using $S_{tumour} = 1$ or 10 and $S_{lymphnode} = 1$. The 25% iso-SAR value (25% of the maximum value in the entire patient) is indicated by the straight dotted line